Colloids and Surfaces B: Biointerfaces 253 (2025) 114733

Contents lists available at ScienceDirect

Colloids and Surfaces B: Biointerfaces

journal homepage: www.elsevier.com/locate/colsurfb

Optimization of aerosolizable and bioactive essential oils-based nanoemulsions: Physico-chemical and biological characterization

Jacopo Forte [a], Eleonora D'Intino [a], Floriana Cappiello [b], Carlo Vetrano [c], Maria Gioia Fabiano [a], Agnese Viscido [d], Maria Grazia Ammendolia [e], Bruno Casciaro [c,*], Federica Rinaldi [a,**], Maria Carafa [a], Maria Luisa Mangoni [c,1], Carlotta Marianecci [a,1]

[a] Department of Drug Chemistry and Technology, Sapienza University of Rome, Rome, Italy
[b] Department of Environment and Health, Mechanisms, Biomarkers and Models Section, Genome Stability Group, Istituto Superiore di Sanità, Viale Regina Elena 299, Rome 00161, Italy
[c] Department of Biochemical Sciences, Laboratory Affiliated to Istituto Pasteur Italia-Fondazione Cenci Bolognetti, Sapienza University of Rome, Rome 00185, Italy
[d] Microbiology and Virology Unit, Sapienza University Hospital "Policlinico Umberto I ", Italy
[e] National Center for Innovative Technologies in Public Health, Istituto Superiore di Sanità, Rome 00161, Italy

ARTICLE INFO

Keywords:
Drug Delivery
Nanoemulsions
Essential oil
Antimicrobial activity
Gram-negative bacteria

ABSTRACT

Antibiotic resistance is one of the major threats to public health, with an increasing number of deaths annually and respiratory tract infections are considered a leading cause of global death, particularly in vulnerable populations. It is therefore extremely urgent to find new therapeutic strategies to overcome this problem and one of these is represented by the design of aerosolizable nanoformulations (NEs). In this work we designed NEs composed by a mixture of *Rosmarinus officinalis* and *Thymus vulgaris* essential oils aiming to obtain an active nanocarrier capable and useful to entrap different active compounds. The formulation, NEs-1, was deeply characterized in terms of dynamic light scattering, ζ-potential measurements, stability studies, antimicrobial activity and cytotoxicity. Our results showed that NEs-1 exhibited useful physico-chemical properties for nose-to lung applications, as well as significant biological activity. However, at the selected oil concentration, it induced cytotoxic effects on eukaryotic cells. We subsequently identified the optimum oil concentration, and the formulation was then optimized to obtain NEs-2, nanoemulsions with similar physico-chemical properties to NEs-1. NEs-2 was furthermore characterized by morphological analysis, in terms of resistance to nebulization process and stability in simulated biological fluid such as nasal and artificial sputum. Moreover, NEs-2 demonstrated the ability to slow down the growth of *E. coli* and *K. pneumoniae*, confirming its potential as a bioactive carrier with the aim of encapsulating antimicrobial molecules and increasing their effectiveness and reducing their adverse effects.

1. Introduction

Antimicrobial resistance (AMR) is a global burden, and it is considered a silent pandemic; it occurs when microorganisms no longer respond to antimicrobials, rendering these specific treatments ineffective [1]. In 2019, AMR provoked over 4.95 million deaths worldwide, and it is estimated that it will cause an economic burden of US$1 trillion in additional healthcare costs by 2050 [2].

Respiratory tract infections are the most common types of infections worldwide, affecting millions of people each year and accounting for an estimated 116 million office visits and 3 million visits to hospital emergency departments [3]. It is evident that antimicrobial-resistant respiratory tract infections are becoming an increasingly public health issue and a leading cause of global death, particularly in vulnerable

* Correspondence to: Department of Biochemical Sciences "A. Rossi Fanelli", Sapienza University of Rome, Piazzale Aldo Moro 5, Rome 00185, Italy.
** Correspondence to: Department of Drug Chemistry and Technologies, Sapienza, University of Rome, Piazzale Aldo Moro 5, Rome 00185, Italy.
E-mail addresses: jacopo.forte@uniroma1.it (J. Forte), eleonora.dintino@uniroma1.it (E. D'Intino), floriana.cappiello@iss.it (F. Cappiello), carlo.vetrano@uniroma1.it (C. Vetrano), mariagioia.fabiano@uniroma1.it (M.G. Fabiano), a.viscido@policlinicoumberto1.it (A. Viscido), maria.ammendolia@iss.it (M.G. Ammendolia), bruno.casciaro@uniroma1.it (B. Casciaro), federica.rinaldi@uniroma1.it (F. Rinaldi), maria.carafa@uniroma1.it (M. Carafa), marialuisa.mangoni@uniroma1.it (M.L. Mangoni), carlotta.marianecci@uniroma1.it (C. Marianecci).
[1] Equally contributed.

https://doi.org/10.1016/j.colsurfb.2025.114733
Received 20 February 2025; Received in revised form 9 April 2025; Accepted 22 April 2025
Available online 29 April 2025
0927-7765/© 2025 The Author(s). Published by Elsevier B.V. This is an open access article under the CC BY license (http://creativecommons.org/licenses/by/4.0/).

populations such as young children, the elderly, and those with weakened immune systems [4].

The World Health Organization (WHO) has published a list of antibiotic-resistant priority pathogens, most of which are represented by Gram-negative bacteria [5] such as *Escherichia coli, Acinetobacter baumannii, Pseudomonas aeruginosa*, and *Klebsiella pneumoniae*. Numerous efforts are being made to overcome the problem of antibiotic resistance, including the use of drug combinations, the production of novel narrow-spectrum antibiotics, and the use of nanotechnology [6,7].

Essential oils (EOs) are aromatic, volatile liquids obtained from plant material through steam distillation [8].

EOs have been studied over the years for several pharmacological properties, such as their antioxidants and antimicrobial properties.

The antimicrobial effects of essential oils vary significantly, often depending on their chemical composition and concentration. Additionally, the mechanism of antimicrobial action can differ based on the specific type of essential oil and the microorganism strain involved [9].

EOs and their bioactive compounds have a low potential to develop microbial resistance due to their multicomponent nature and their multi-target activity against MDR (multidrug resistant) bacteria.

Moreover, due to their complex mixtures, researchers have proposed several synergistic mechanisms for EOs-antibiotic combinations, including the inhibition of efflux pumps, blocking the production or activity of specific enzymes (such as beta-lactamases, lipases, and coagulases), and disrupting bacterial membranes by impairing ATPase activity [10].

An effective strategy for treating infections could be the use of bioactive nanocarriers (with antimicrobial activity), composed of EOs, capable of entrapping, delivering and releasing a specific drug, protecting it from degradation and increasing its bioavailability. In this way, the carrier itself could be active and subsequently enhance the activity of the active delivered molecules [11].

Nanoemulsions (NEs) are nanocarriers composed of essential oil, able to entrap and deliver several active compounds. They are easy to prepare, and they are generally considered as safe [12]. Due to their small dimensions, NEs are expected to provide an efficient delivery of therapeutic agents in a targeted manner. Furthermore, NEs can effectively represent a bioactive drug delivery system as the oily component used may possess intrinsic biological activity [13].

In this study, NEs have been formulated using a mixture of essential oils: *Rosmarinus officinalis* L. essential oil (REO) and *Thymus vulgaris* L. essential oil (TEO). It is known that REO can enhance the antimicrobial activity of Ciprofloxacin against *Klebsiella pneumoniae* at specific concentrations [14], while TEO has a strong ability to inhibit and eradicate biofilm, reducing the concentration of antibiotic conventionally used [15]. Thymus species are of particular interest for investigating natural antimicrobial agents and exploring the potential synergistic effects with conventional drugs, mainly due to their rich content of bioactive compounds and strong antimicrobial activity [16]. Recent studies have demonstrated that TEO significantly enhances the antimicrobial activity of conventional antibiotics. This synergistic effect suggests promising potential for utilizing EOs in conjunction with antimicrobial medications to tackle the emergence of multidrug-resistant bacteria [17].

In the context of respiratory tract infections, one promising strategy could be the administration of bioactive NEs, composed by REO and TEO, directly into the lungs via aerosolization to enhance therapeutic effects and perform superior targeting. In fact, inhalable nanoformulations for treating lung diseases allow for precise pulmonary drug delivery, overcoming physiological barriers, improving aerosol lung deposition rates, and increasing drug bioavailability. These formulations hold great potential in facing the challenges in treating lung diseases [18].

The aim of this work is to design NEs characterized by low cytotoxicity and with antimicrobial activity. This was achieved through a multidisciplinary approach that enabled us to impart the suitable chemical-physical characteristics and composition to the NEs. A multidisciplinary approach is pivotal in the development of nanocarriers, as it facilitates the integration of diverse scientific expertise necessary to address the complex challenges involved in designing effective drug delivery systems. To ensure the *in vivo* effectiveness of nanocarriers, it is essential to optimize not only their chemical and physical properties but also to study, and try to predict, their interactions with biological systems. The designed NEs are intended to serve as effective carriers for active molecules, such as conventional antibiotic or small bioactive peptides (e.g., antimicrobial peptides) enhancing their stability, solubility, bioavailability and efficacy. By carefully selecting the qualitative and quantitative components of the formulation, including surfactants and oils, the goal is to achieve a bioactive delivery system for pulmonary applications, making NEs a valuable tool and a versatile platform in pharmaceutical and therapeutic formulations.

2. Materials and methods

2.1. Materials

Tween® 85, Rosemary oil (*Rosmarinus officinalis* L. essential oil), Thyme oil (*Thymus vulgaris* L. essential oil), Diphenylhexatriene (DPH), Ethanol and Hepes salt [N-(2-hydroxyethyl)piperazine-N′-(2-ethanesulfonic acid)] were purchased by Sigma-Aldrich (St. Louis, MO, USA). Mueller Hinton (MH) broth was purchased by Sigma-Aldrich (St. Louis, MO, USA), while Mueller Hinton II was from BD (Le pont de Claix, FR). Artificial sputum medium was purchased from Biochemazone (Leduc, AB, Canada).

Simulated nasal fluid was prepared by dissolving 7.45 mg/mL NaCl, 1.29 mg/mL KCl, and 0.32 mg/mL $CaCl_2 \cdot 2\ H_2O$ in distilled water.

2.2. Pseudo-ternary phase diagram construction

The pseudo-ternary phase diagram, consisting of *Thymus vulgaris* L. essential oil (TEO), *Rosmarinus officinalis* L. essential oil (REO), Tween® 85 and Hepes Buffer (10^{-2} M, pH 7.4) was constructed. The oil phase was composed of a mixture of two different essential oils (EOsMIX), TEO and REO, in a precise volume ratio (% v/v), as represented in Table 1. The higher amount of TEO oil with respect to REO ratio is due to its stronger antimicrobial activity, as suggested by preliminary studies reported in Fig. S1 and S2 and according to what previously reported by Miladi et al. [19].

The mixtures were obtained by combining specified amounts of surfactant, oil phase (EOsMIX), and aqueous phase in various weight ratios within a test tube, followed by vigorous vortexing for two minutes to ensure thorough mixing.

These mixtures were then plotted on a two-dimensional horizontal surface, conventionally represented as an equilateral triangle, where each vertex indicates 100 % of one component and 0 % of the others. Each side of the triangle corresponds to the weight/weight (w/w) percentage of the components, and every point within the diagram reflects a unique quantitative composition.

After preparing each sample, visual inspection was conducted to classify the emulsions as either "homogeneous" or "non-homogeneous." An emulsion was deemed homogeneous if there were no visible particle growth or phase separation, indicating stability. In contrast, non-homogeneous dispersions appeared highly turbid with clear phase separation of the components.

All points representing the prepared formulations were added to the diagram, delineating two areas corresponding to the visually classified

Table 1
EOs_{MIX} composition.

TEO (%)	REO (%)
66	34

homogeneous and non-homogeneous emulsions. From the pseudo-ternary phase diagram showing the homogeneous region, several nanoemulsions with varying compositions were selected for analysis. These chosen formulations underwent a physicochemical stability test.

2.2.1. Preparation of nanoemulsions

From the obtained homogeneity region of the pseudo-ternary phase diagram, a sample (NEs-1) was selected. The selected ratio of EOs_{MIX}, surfactant and water, reported in Table 2, was vortexed for about 2 minutes to allow micro-emulsion to form, and then, the obtained microscale droplets were sonicated for 1 minute at 25 °C, using a tapered microtip operating at 20 kHz at an amplitude of 20 % (Vibracell-VCX 400, Sonics, Taunton, MA, USA).

At this stage, the formulation can be sterilized by using cellulose filters (0.22 μm) in accordance with Ph. Eur.

A schematic cartoon of the preparation method has been provided in Supplementary Material section (Fig. S3).

Based on the preliminary results obtained, to overcome cytotoxicity limitations related to NEs-1 composition, an appropriate combination of oil mixture/surfactant/water was selected for further experiments (NEs-2). The selected ratio of EOs_{MIX}, surfactant and water are reported in Table 2, and the preparation method is the same as described previously but the obtained microscale droplets were sonicated for 3 minutes at 25 °C, using a tapered microtip operating at 20 kHz at an amplitude of 20 % (Vibracell-VCX 400, Sonics, Taunton, MA, USA).

2.3. Dynamic light scattering and ζ-potential measurements

The hydrodynamic diameter and polydispersity index (PDI) of the prepared NEs were assessed at 25 °C by using a ZetaSizerNano 90S (Malvern Instruments Ltd., Worcestershire, United Kingdom), equipped with a 5 mW HeNe laser (wavelength λ = 632.8 nm) and a digital logarithmic correlator. Normalized intensity autocorrelation functions were detected at a 90° angle and analyzed using a Contin algorithm to determine the decay time of the electric field autocorrelation functions. By utilizing the decay time, the distribution of the diffusion coefficient D of the particles could be obtained. With the Stokes–Einstein relationship (RH = KBT/6πηD, where KBT represents thermal energy and η represents solvent viscosity), the effective hydrodynamic radius RH was calculated. The reported values of the radii in this study correspond to the intensity-weighted average [20].

The absolute ζ-potential value of the NEs was determined by measuring electrophoretic mobility using the Smoluchowski equation ζ = uη/ϵ, where η and ϵ denote the viscosity and the permittivity of the solvent phase.

2.4. Oil droplet characterization by DPH: fluorescence anisotropy

Oil droplet features were examined using a lipophilic fluorescent probe: DPH, which provides information about fluidity of the oil nanodroplets.

Specifically, DPH-loaded NEs were formulated by evaporating DPH solution at a concentration of $2 \cdot 10^{-4}$ M to obtain the dry powder to be mixed with EOs, and then vortexed [21].

The surfactant and Hepes buffer were then added, resulting in a microemulsion vortexed and sonicated as previously described.

DPH measurements were performed with excitation λ_{ex}: 400 nm and detecting the fluorescence intensity at λ_{em}: 425 nm, using a luminescence spectrometer (LS5013, PerkinElmer, Waltham, MA, USA).

The fluorescence anisotropy (A) was calculated using the following ratio:

$$Fluorescence\ anisotropy(A) = \frac{(I_{vv} - I_{vh}) \bullet G}{(I_{vv} + 2 \bullet I_{vh}) \bullet G}$$

Where the G factor is the ratio of sensitivity of the detection system, expressed as I_{hv}/I_{hh} ratio. I_{vv}, I_{vh}, I_{hv} and I_{hh} are the intensities (λex: 350 nm, λem: 428 nm) of the fluorescence measured by a LS5013 PerkinElmer spectrophotometer with *v* (vertical) and *h* (horizontal) orientation of the polarized light.

Table 2
NEs-1 and NEs-2 composition.

Sample	EOs_{MIX} (mg/mL)	Tween® 85 (mg/mL)	EOs_{MIX} tested (mg/mL)*
NEs−1	340	200	15
NEs−2	4.68	3.12	0.12

* The highest concentration tested in the biological assays

2.5. Optical and electronic microscope observations

Optical microscopic visualization of samples was performed by dark field microscope. Glass slides were cleaned by submerging in 70 % ethanol solution and allowed to air dry for approximately five minutes. A 10 microL of the samples were put on cleaned slides, coated with a coverslip and immediately observed. Dark field microscope images were scanned under a 40X objective and taken using an Olimpus BX53 microscope (Waltham, MA, USA) equipped with a Tucsen Camera GT H series and Tucsen ISCapture 5.1.1 software.

To reveal the morphological aspect of the optimized nanoemulsions (NEs-2), transmission electron microscope (TEM) was used. A drop of sample was placed on a copper grid (400 mesh) containing a Formwar ultrafilm, stained with 2 % phosphotungstic acid solution and kept for drying at room temperature before loading under the microscope (Fei 208S, FEI Company, Hillsboro, OR, USA). Sample visualization was performed by using a Mega-view II SIS camera (Olympus, Microscopy Technologies, Tokio, Japan) at an accelerating voltage of 100 kV. Collected images were processed by Adobe Photoshop (CS5 version) (San Jose, CA, USA) for editing.

2.6. Stability studies

Stability studies were performed on both NEs-1 and optimized NEs-2, monitoring possible variations in hydrodynamic diameter and ζ-potential over time. These experiments are conducted using DLS (Malvern Instruments, Worcestershire, UK). The stability of the samples was evaluated for 90 days at room temperature and 4 °C.

2.7. Biological evaluation

2.7.1. Bacterial strains and cell lines

The Gram-negative *E. coli* 25922 (from the American Type Culture Collection, ATCC) and the clinical isolate *K. pneumoniae* #17 (from the strain collection of Policlinico Umberto I, Sapienza, University of Rome) were used to test the antimicrobial potency of the designed formulation. The cytotoxic effect of nanoemulsions was evaluated against the human type II alveolar epithelial cells (A549, from ATCC). They were cultured in Dulbecco's modified Eagle's medium (DMEM) supplemented with 2 mM glutamine (DMEMg), 10 % heat-inactivated fetal bovine serum (FBS), and 0.1 mg/mL of penicillin and streptomycin, and incubated in 25 cm^2 or 75 cm^2 flasks at 37 °C and 5 % CO_2.

2.7.2. Stability of nanoemulsions in culture media

As a preliminary biological evaluation, the *in vitro* stability of nanoemulsions in the presence of MH, MH-II and DMEM culture media has been carried out. Both NEs-1 and NEs-2 were diluted in culture media to obtain a final concentration of 45 %. The average size, polydispersity index, and ζ-potential were evaluated by means of DLS maintaining samples at 37 °C and performing measurements at different time points (every hour for the first 8 hours, and then until up to 24 h).

After NEs-1 optimization in terms of components amount, NEs-2 stability was also evaluated in Simulated Nasal Fluid (SNF) and in Artificial Sputum Medium (ASM, that mimics real human sputum

containing lipids, micronutrients, amino acids, mucin, proteins, and free DNA) at 34 °C and 37 °C, respectively, to assess NEs-2 integrity and stability imagining their administration via inhalation. Simulated nasal fluid was prepared according to Tanigawa et al., 2022 [22].

Mixtures of NEs-2 and 50 % ASM and simulated nasal fluid were prepared and incubated at their respective temperatures. Analyses were performed at different time intervals (0, 5, 10 and 15 minutes for simulated nasal fluid and 0, 1, 2, and 3 h for ASM) by DLS (Nano ZS90, Malvern, UK) to evaluate possible variations of particle size, ζ-potential, and polydispersity index and the resistance of nanoformulations at these media.

2.7.3. Cell viability assay

The cytotoxicity of NEs (NEs-1/NEs-2) were evaluated by the colorimetric 3-(4,5-dimethylthiazol-2-yl)-2,5-diphenyltetrazolium bromide (MTT) assay.

The cells, resuspended in DMEMg plus 2 % FBS, were plated in each well of 96-well plates (approximately 4×10^4 per well) and then incubated at 37 °C and 5 % CO_2 for 24 h. After overnight incubation, the medium was replaced with 100 µl of DMEMg containing the NEs at different concentrations.

The plate was incubated for 24 h at 37 °C in a 5 % CO_2 atmosphere and then the medium was replaced with Hank's buffer (136 mM NaCl; 4.2 mM Na_2HPO_4; 4.4 mM KH_2PO_4; 5.4 mM KCl; 4.1 mM $NaHCO_3$, pH 7.2, supplemented with 20 mM d-glucose) containing 0.5 mg/mL MTT. The plate was incubated for 4 h and the formed formazan crystals were dissolved by adding 100 µl of acidified isopropanol. The cell viability was determined by absorbance measurements at 570 nm using a microplate reader (Infinite M200; Tecan, Salzburg, Austria) and calculated with respect to the control (untreated cells).

2.7.4. Antimicrobial assay

The antimicrobial efficacy of the designed NEs (NEs-1/NEs-2) was evaluated *in vitro* by monitoring the microbial growth of two different Gram-negative bacteria, i.e. *E. coli* and *K. pneumoniae*.

In particular, NEs-1 was firstly tested at different serial two-fold concentrations against *K. pneumoniae* in a microdilution broth assay. Briefly, bacteria were grown in Luria-Bertani (LB) broth at 37 °C until an optical density (OD) of 0.8 was reached. The bacteria were then diluted in MH-II and added to each well of a 96-multi well plate containing the diluted NEs (final cell concentration of 1×10^6 cells/mL). The plate was incubated for 16 h at 37 °C and microbial growth was evaluated by measuring the OD at 590 nm using a microplate reader (Infinite M200; Tecan, Salzburg, Austria).

The optimized NEs-2 at its optimal non-cytotoxic concentration, was tested as reported above against both *E. coli* and *K. pneumoniae* and in two different media, MH and MH-II.

2.8. Nebulization studies

Simulated nebulization process conducted by a jet nebulizer can provide information on the NEs resistance to this administration process. NEs aerosols were generated by using a jet nebulizer (Nebula Air Liquide Medical Systems S.p.A., Bovezzo, Italy).

A volume of 5 mL of the sample was used, and the aerosolized NEs-2, then called NEs-2 (post), was collected in the collecting tube.

Nebulizers generally operate to dryness, the point at which no further useful aerosol is generated, even if some residual fluid always remains in the nebulizer reservoir. Therefore, the total mass output of the sample tested was always less than 100 %. After nebulization to dryness (10 min), NEs-2 was analyzed in terms of size, PDI and ζ-potential to evaluate the effect of nebulization process on NEs physicochemical features and investigate their resistance to this type of administration.

3. Results and discussion

3.1. Pseudo-ternary phase diagram construction

The pseudo-ternary phase diagram (Fig. 1) of EOs_{MIX}, Tween® 85, and Hepes buffer (as the aqueous phase) was constructed, allowing for the identification of homogeneous and non-homogeneous phase regions.

This enabled the selection of a suitable composition of the NEs formulation. The homogeneous region is marked in blue.

A specific sample (NEs-1) was chosen from this area to achieve a final formulation with desired properties, such as optimal particle size and ζ-potential, which are essential for developing a carrier suitable for nose-to-lung delivery.

Notably, the surfactant concentration was specifically selected to stabilize the oil nanodroplets in water composed by a high amount of oil phase.

3.2. Physical-chemical characteristics of NEs-1

In Table 3 the physical-chemical features of NEs-1 in terms of hydrodynamic diameter, polydispersity index (PDI) and ζ-potential were reported. Moreover, the hydrodynamic diameter, autocorrelation function, intensity distribution/ζ-potential distribution plots have been reported in Fig. S4. Smaller droplet sizes are generally preferred for pulmonary administration, as they can enhance deposition in the alveolar region. The optimal formulations have droplet sizes below 200 nm, which is ideal for deep lung penetration [23,24].

The sample NEs-1 is characterized by a size of approximately 170 nm, making it potentially optimal for a nose-to lung application. Regarding the ζ-potential value, it reflects the surface charge of nanoemulsions. A higher absolute ζ-potential (around or > 30 mV) suggests a potential stability of the soft nanocarrier over time due to electrostatic repulsion among droplets [25,26].

In particular, the NEs-1 was characterized by a ζ-potential of −31 mV, useful to ensure a potential stability of the sample over time, reducing the risk of droplet aggregation. In Table 3 it is also reported that the PDI (Polydispersity Index) value of the NEs-1 (0.13 ± 0.01), indicates a relatively narrow size distribution of the nanoemulsions. A PDI value below 0.2, suggests that the nanoemulsions are uniform in size [27,28]. The nanoemulsions of a monodisperse sample, characterized by a uniform particle size, are likely to exhibit optimal *in vivo* biodistribution, thereby enhancing the targeted delivery and bioavailability of the encapsulated active compounds. Additionally, a narrow size distribution minimizes the risk of aggregation, which is essential for

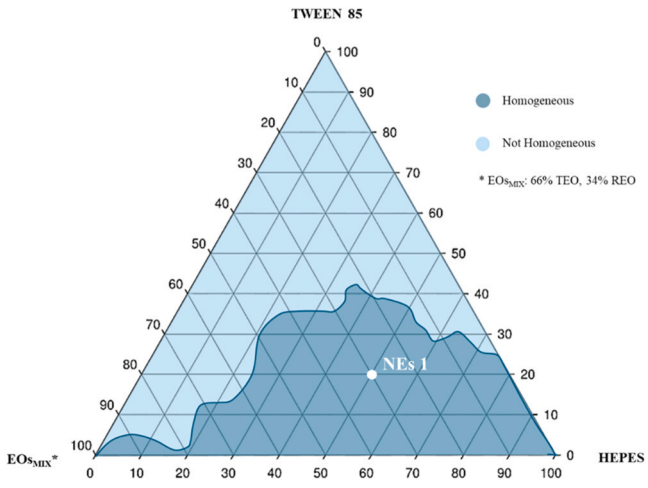

Fig. 1. Pseudo-ternary phase diagram of EOs_{MIX}, Tween® 85 and Hepes Buffer: the homogeneous phase (dark blue area) and the not homogeneous phase (light blue area) NEs-1 composition has been chosen into the homogeneous region.

Table 3
Physical-chemical features of NEs-1 in terms of hydrodynamic diameter, polydispersity index (PDI), ζ-potential and anisotropy value.

Sample	Hydrodynamic diameter ± SD (nm)	PDI ± SD	ζ-potential ± SD (mV)	Anisotropy A. U. (Fluidity)
NEs−1	176.00 ± 0.91	0.13 ± 0.01	−31.40 ± 1.69	0.17

maintaining stability over time of the sample [29]. In summary, the PDI value of 0.13 ± 0.01 of NEs-1 reflects a well-optimized formulation.

In addition, oil drop characterization in terms of anisotropy has also been carried out. This feature in fact, is crucial to predict the capability of the sample to interact with cells/bacteria membranes or to release the loaded drug. Due to the hydrophobic nature DPH was localized into the oil drop of the NEs and could give information about the droplet rigidity/fluidity.

A NEs exhibiting an anisotropy value of 0.17 (Table 3) can be classified as a highly fluid nanocarrier [30], suggesting a greater potential for content release and the likelihood of interaction with biological membranes.

Their low anisotropy values suggest they may interact effectively with cells, facilitating rapid release of their payload for immediate local therapeutic action.

3.3. Physical-chemical stability

The results of NEs-1 stability studies, carried out at room temperature (25 °C) and 4 °C, were reported in Fig. 2. From Fig. 2, left, it is possible to observe the variation of nanocarrier's properties (droplet size and ζ-potential) at storage conditions of room temperature. Typically, room temperature could lead to accelerated degradation or aggregation of nanoemulsions resulting in larger droplet sizes and potential instability. Despite this, the NEs-1 stored at room temperature shows minimal and not significant change in hydrodynamic diameter (on the 90 day), this suggests that NEs-1 was characterized by suitable stability in this storage condition (until up to 60 days). Probably the fairly negative ζ-potential preserves the sample from significant coalescence phenomena [26].

A similar behavior characterizes the NEs-1 stored at 4 °C (Fig. 2, right). Despite these hydrodynamic diameter slight changes at 90 days, it can be concluded that the formulations stored at both temperatures remain relatively stable, as the slight increase in size does not compromise its overall performance [31]. Probably, for NEs-1 the ideal storage duration is 60 days.

NEs stability in the media employed for the *in vitro* studies, with both eukaryotic and prokaryotic cells, is crucial for ensuring reliable results.

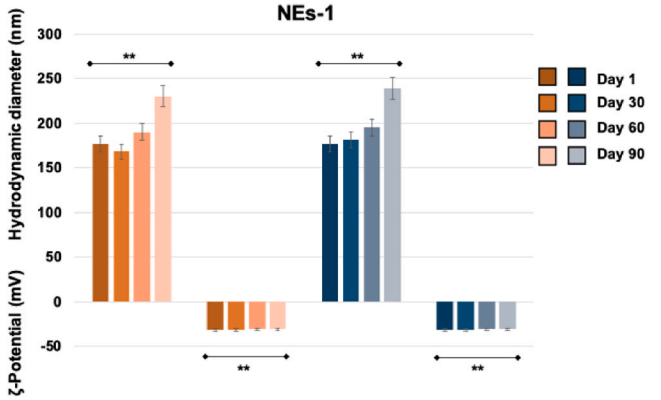

Fig. 2. Stability studies over time of NEs-1 at Room Temperature (25 °C) (left) and 4 °C (right). Data were obtained as the average of three independent experiments. * $p < 0.05$, * * $p < 0.01$, * ** $p < 0.001$.

When nanoemulsions are in contact with culture media, they may interact with proteins, salts and other components present in the medium [32].

Fig. 3 shows the trend of hydrodynamic variation of the NEs over 24 h. The experiments were carried out at 37 °C evaluating the NEs-1 size by DLS measurements for 24 h as described in the Material and Methods section. Hydrodynamic diameter appears to be affected by the presence of all culture media, but no significant changes were observed, and it is possible to affirm that the artificial media doesn't influence the NEs integrity.

Probably, the trend in the increased hydrodynamic diameter (MH < MH- II < DMEM) of the NEs-1 could be explained by a partial coating of the nanocarrier surface by culture media components (Table S2) which was different for each of the three media and correlated with the richness of the culture medium.

In fact, MH is a culture medium primarily used for microbiological testing and its composition is relatively simple as it is specifically designed to support the growth of bacteria without interfering with antibiotic susceptibility testing. It is composed primarily of beef extract, starch, minerals and salts (such as sodium chloride) and does not contain high levels of amino acids, vitamins or other advanced nutrients. MH-II is like MH but adjusted with cations (calcium and magnesium).

The DMEM is a much more complex culture medium, containing high concentrations of glucose, amino acids, vitamins, and mineral salts because it is designed to support the growth of a wide range of animal cells that require a wider range of nutrients than bacteria.

3.4. Evaluation of NEs-1 cytotoxicity

The effect of NEs-1 on eukaryotic cell viability was evaluated on the human type II alveolar epithelial A549 cells after 24 hours of incubation at different serial two-fold concentrations of EOs_{MIX}, starting from 15 mg/mL to 0.03 mg/mL. As reported in Fig. 4, NEs showed a high cytotoxicity at the highest concentrations, causing approximately 100 % of cell death. At low concentrations (ranging from 0.12 to 0.03 mg/mL) NEs-1 showed a safe profile, with a slight reduction in cell viability (< 20 %). The cytotoxicity of NEs can be ascribed to the known cytotoxicity that essential oils exhibit at high concentrations and may be due to several mechanisms of action such as (i) induction of cell death by apoptosis/necrosis; (ii) cell cycle arrest; (ii) the loss of key organelles function [19,33].

3.5. Antimicrobial efficacy of NEs-1

NEs-1 was also tested for its antimicrobial activity against *K. pneumoniae* at different serial two-fold concentrations of EOs_{MIX} (i.e, from 15 to 0.03 mg/mL).

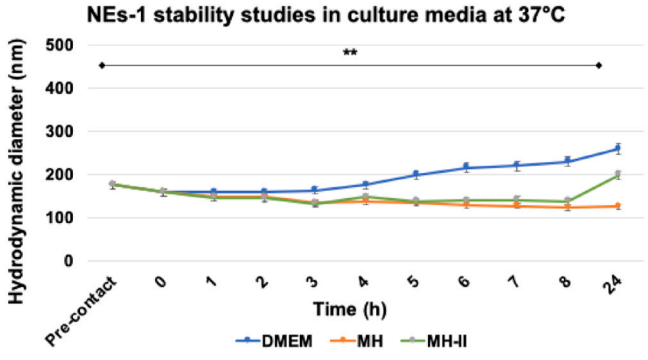

Fig. 3. Effect of different culture media (DMEM, in blue, MH, in red and MH-II, in green) at different incubation times on hydrodynamic diameter of NEs-1. Data were obtained as the average of three independent experiments. * $p < 0.05$, * * $p < 0.01$, * ** $p < 0.001$.

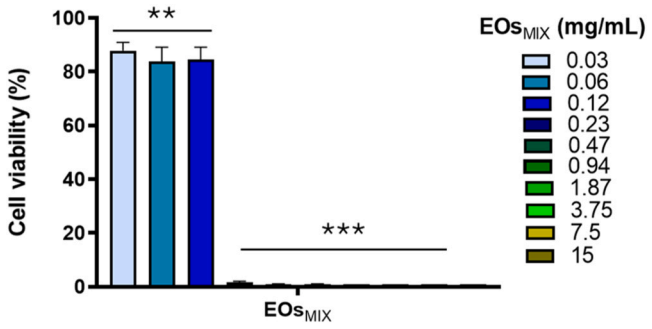

Fig. 4. Evaluation of NEs-1 cytotoxicity by MTT assay. Data represent the mean ± SEM of three independent experiments. Statistical significance between each values versus untread cells (set as cell viability = 100 %) was reported as follow: * * $p < 0.01$, * ** $p < 0.001$.

The microbial growth was monitored in a microplate reader (at 590 nm) and the values of OD are reported in Fig. 5. NEs-1 showed a potent antimicrobial activity causing approximately 100 % of inhibition of microbial growth at high concentrations, which were cytotoxic. Interestingly, a slight antimicrobial activity was observed at the non-cytotoxic concentration of 0.12 mg/mL and therefore this was selected as the optimal non-cytotoxic concentration with antimicrobial activity.

Considering this optimal concentration and the dilution that the sample undergoes in biological evaluation assays (see Table 2), a different composition of NEs was selected by Pseudo-ternary diagram (the same reported in Fig. 1). The selected point is reported in Fig. 6.

3.6. *Pseudo-ternary phase diagram construction and identification of NEs-2*

The development of an efficient nanocarrier involves the optimization of a considerable number of parameters that could impact *in vivo* performance. Therefore, proper design and selection of *in vitro* characterization tools are of crucial importance in gaining an insight into the prospective *in vivo* behavior.

Specific features such as hydrodynamic diameter and ζ-potential, could affect the nanocarrier stability, the release of drug at targeted site, the interaction with cells or bacteria, and its bioavailability *in vivo*.

Fundamental in this work was to prepare NEs-2, characterized by different composition (Table 2) with respect to NEs-1, with the similar physical-chemical characteristics of NEs-1.

The composition of NEs-2 was also selected from within the homogeneity region of the ternary phase diagram, also in accordance with the biological results. Fig. 7 demonstrates the homogeneity/heterogeneity of the pre-sonication samples, both visually and through optical

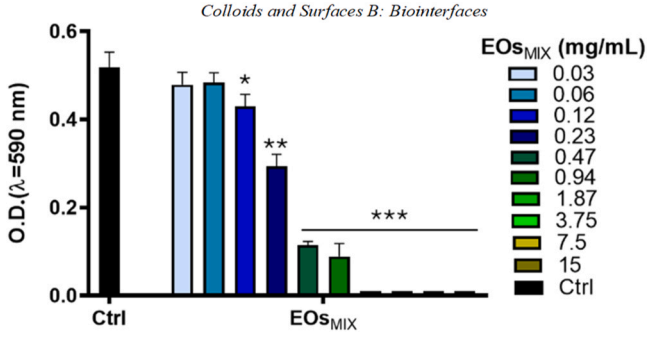

Fig. 5. Antimicrobial activity of NEs-1 evaluated by measuring the microbial growth (optical density, O.D.). Ctrl represents untreated bacteria. The data are the mean ± standard deviation (SD) of three independent experiments. Statistical significance between each value versus the control (Ctrl) was reported as follow: * $p < 0.05$, * * $p < 0.01$, * ** $p < 0.001$.

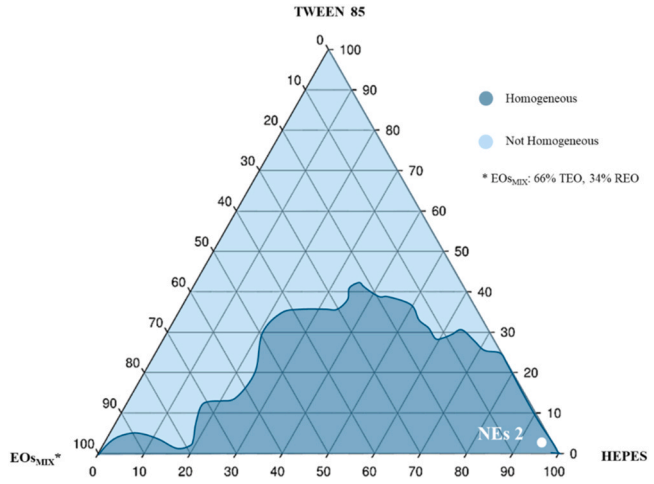

Fig. 6. Pseudo-ternary phase diagram of EOs_{MIX}, Tween 85 and Hepes Buffer. The resulting phases were the homogeneous phase (dark blue area) and the not homogeneous phase (light blue area) The new composition has been chosen into the homogeneous region.

microscopy. To analyze the samples after visual inspection, dark field microscopy was used. Dark field microscopes allow the visualization of particles at micro/nanoscales without the use of chemical dyes and the need for high magnification, due to the principles of refraction and reflection. Dark field works based on the observation of the specimen by light from a condenser. The light beam falls directly on the sample, but refractively. So, the light will touch the sample making it bright against a dark background, but only a part of the light will pass obliquely. This light is diffracted, refracted and reflected into the lens. The combination of these lenses allows to produce significant image amplification values. In dark-field observation, the membrane of droplets can be observed in high contrast, since membranes between the oil phase and the aqueous phase look bright against the dark background. Fig. 7 shows a combination of images from visual inspection and dark-field microscopy. The sample A as shown in the figure, exhibits clear phase separation at visual inspection. Also, the analysis in dark field of the aqueous phase reveals significant inhomogeneity in its external structure, suggesting a non-uniform distribution of the components. Sample B, which appeared homogeneous upon visual inspection, in dark-field observations showed many large oil droplets (thin arrows) along with a high number of water/oil/water aggregates (small arrows) dispersed among micro and nanostructure. Finally, Sample C, which was homogeneous upon visual inspection, also appeared homogeneous in dark-field observations with finely dispersed nanostructure and few small oil droplets. Dark field microscopy, especially for samples B and C, confirms what was observed through visual inspection, namely that the samples selected in the pseudo-ternary phase diagram are homogeneous in terms of phase separation and are capable, when subjected to a high-energy process (sonication), of producing stable nanoemulsions.

NEs-2 has been prepared with the same method of NEs-1, but to obtain the same range of size, ζ-potential, and PDI reported in Table 3,

it has been necessary to prolong the sonication time (see M&M section) [34].

Indeed, it is well known that prolonged exposure of emulsions to sonication results in a reduction of droplet sizes, generating high-energy force that leads to the formation of nano-sized droplets [34].

In particular, NEs-2 contains a lower amount of oil compared to NEs-1 and when the oil content is reduced, more energy input (in this case 3 minutes of sonication instead of 2 minutes) is required to break the oil nanodroplet into smaller nanostructure and achieve a comparable size between NEs-1/2. This is because with less oil content present, the dispersion process becomes less efficient, so higher energy inputs are needed to achieve the desired droplet size (from 230 nm to 163 nm, see

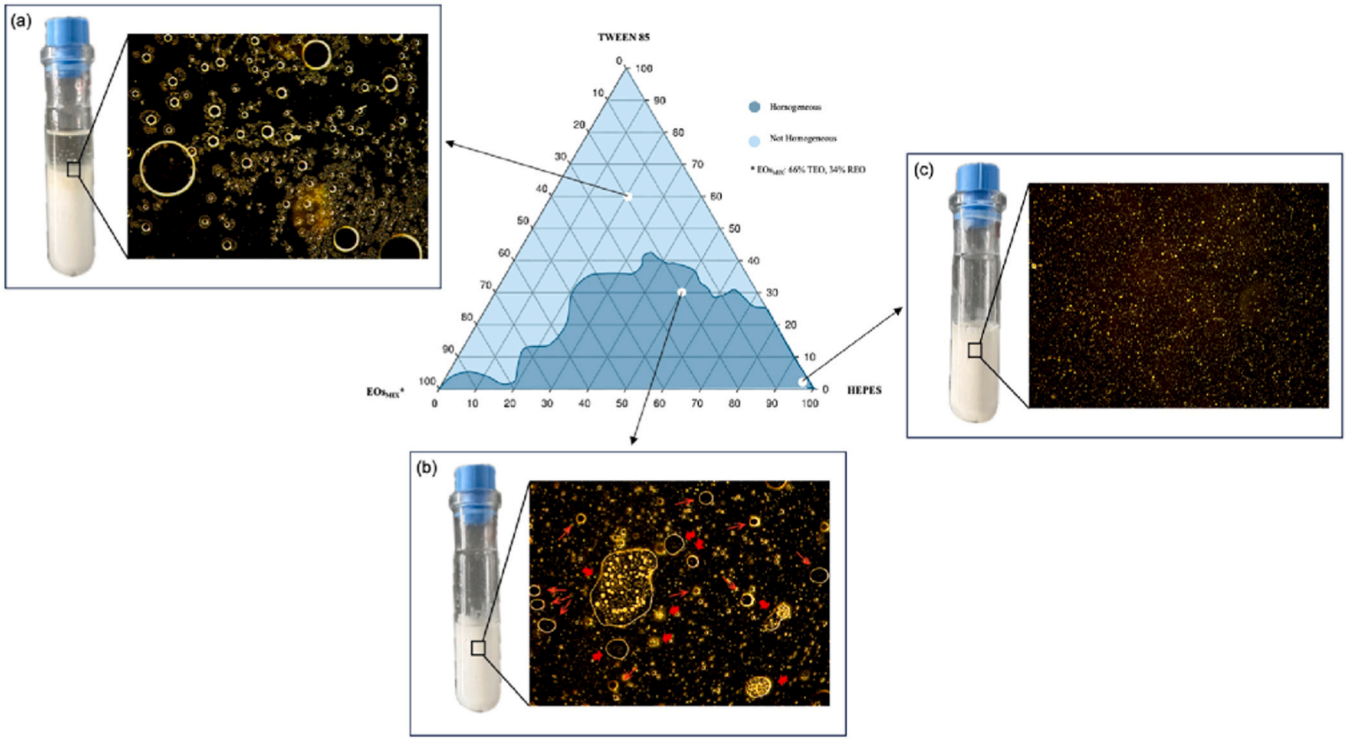

Fig. 7. Visual inspection and optical microscope observations of samples included in homogeneous/non-homogeneous area of ternary diagram.

Supplementary Materials, Table S1) [35]. Of the selected sample (NEs-2), oil droplet characterization in terms of anisotropy was also carried out. In fact, considering the biological efficiency of NEs-1, it was crucial that the anisotropy value of NEs-2 was similar.

As shown in Table 4, the anisotropy value of NEs-2 (0,13 A.U.) is very similar and around the same range as that of NEs-1 (0,17A.U.).

All these data confirm that the slight modifications made to the preparation method resulted in the production of NEs-2, which is very similar to NEs-1 in terms of Hydrodynamic diameter, PDI, ζ-potential, and Anisotropy.

3.7. Morphological analysis

TEM images, shown in Fig. 8, revealed the nanoemulsions as almost spherical particles with no signs of coalescence. Most droplets appeared with sizes in agreement with the DLS analysis. The magnified area of the identified region in the representative image of the Fig. 8 (right panel) revealed that the globules exhibited a compact and homogeneous structure without ultrastructural discontinuities in the surface texture.

3.8. NEs-2 stability studies

NEs-2 was also characterized in terms of long-term stability and stability in the biological fluids (the same previously used to characterize NEs-1). It can be observed that, with respect to NEs-1, NEs-2 demonstrates stability at both tested storage temperatures (Fig. 9) up 90 days. Probably, this enhanced stability could be explained by the different NEs-2 composition in terms of surfactant amount with respect to essential oil.

In particular, NEs-1 is characterized by higher surfactant

Table 4
Physical-chemical features of NEs-2 in terms of hydrodynamic diameter, polydispersity index (PDI), ζ-potential and anisotropy value.

Sample	Hydrodynamic diameter ± SD (nm)	PDI ± SD	ζ-potential ± SD (mV)	Anisotropy A. U. (Fluidity)
NEs−2	163.70 ± 4.25	0.13 ± 0.01	−27.60 ± 2.81	0.13

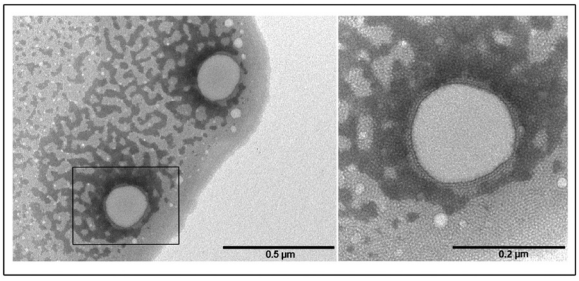

Fig. 8. Optimized nanoemulsions (NEs-2) visualized in transmission electron microscopy by negative staining.

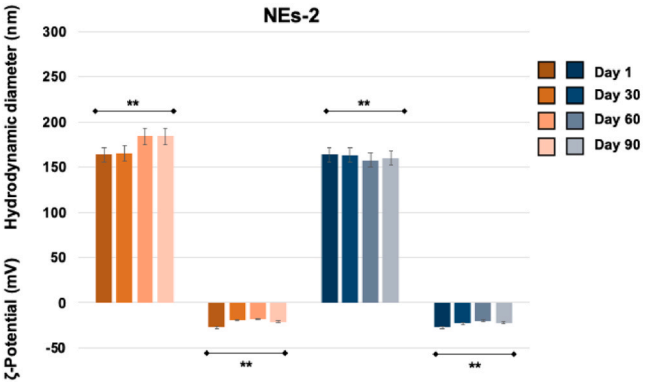

Fig. 9. Stability studies over time of NEs-2 at Room Temperature (25 °C) (left) and 4 °C (right). Data were obtained as the mean of three independent experiments. * $p < 0.05$, * * $p < 0.01$, * ** $p < 0.001$.

concentration, compared to NEs-2 and with respect to the amount of essential oil mix. Related to this, several studies indicated that raising the surfactant concentration could compromise long physical stability by leading to the formation of different types of aggregates [36].

Furthermore, the stability of NEs-2 follows a comparable trend with respect to NEs-1 in the culture media (employed in in vitro biological evaluation: MH, MH II, DMEM) in terms of hydrodynamic/ζ-potential variations (Fig. 10 panel a).

Based on these observations, it can be concluded that NEs-2 also demonstrates stability in these media.

To develop a nanocarrier with potential for nasal administration, it is crucial to assess its stability within artificial environments that can mimic the biological fluids encountered during this delivery.

For this purpose, according to experiment carried out with NEs-1, stability of NEs-2 was evaluated in SNF (which simulates the environment within the nose) and ASM (which simulates the environment within the deeper regions of the respiratory tract) at specific temperature to mimic *in vivo* conditions and the results were reported in Fig. 10 (panel b-c).

In particular, the stability studies performed focus on assessing changes in the physicochemical properties of NEs-2, such as particle size. The data presented in Fig. 10 (panels b-c) show that the sample

does not exhibit significant variations in hydrodynamic diameter. In conclusion, it can be stated that the sample demonstrates resistance to both media employed in the experiments and could be suitable for nasal-lung administration.

The newly designed NEs-2 was tested for its capability to inhibit the growth of two different Gram-negative bacteria, i.e., *E. coli* ATCC 25922 and the clinical isolate *K. pneumoniae* #17. The growth was monitored for 16 hours and reported as O.D. (lambda = 590 nm). As reported in Fig. 11, the formulation showed moderate capability to slow down microbial growth, as proved by the lower O.D. obtained after 16 h of incubation.

In particular, NEs-2 at 0.12 mg/mL was able to reduce the growth of *K. pneumoniae* in both MH and MH-II media with respect to the control (blue lines vs red line, respectively).

Similar effect was observed for *E. coli* in MH-II with a milder effect in MH. These data confirm the moderate antimicrobial potency of empty NEs-2, previously found also for NEs-1. Furthermore, the safety profile of NEs-2 was also confirmed by evaluating eukaryotic cell viability as reported above and the formulation was found to be free from cytotoxic effects (cell viability = 97.562 % ± 2.293) at its optimal concentration (i.e., 0.12 mg/mL), as previously obtained.

3.9. Nebulization studies

In view of possible administration by pulmonary route, the samples were nebulized to test compatibility with the hypothesized administration method. The evaluation of hydrodynamic diameter, PDI and ζ-potential values has been repeated after nebulization (Table 5).

This investigation is relevant in order to evaluate whether nebulizers can disrupt the nanodroplet, thus causing a marked loss of the hypothetically entrapped drug. NEs-2 does not undergo any relevant variation of physicochemical features, suggesting its integrity after the nebulization process. All these preliminary findings can suggest that NEs-2 formulation could be resistant to nebulization stress thanks to its high charge, despite the fluidity feature of the nanodroplet. Moreover, considering the nasal administration route, the prepared and characterized nanoemulsions, due to their specific features, could reach the deeper regions of the lungs [36].

4. Conclusions and future perspectives

Multidrug-resistant respiratory infections represent a serious public health problem and new strategies to combat this threat are urgently needed. In this work, we designed a bioactive essential oils-based nanoemulsions by combining *Rosmarinus officinalis* and *Thymus vulgaris* essential oils.

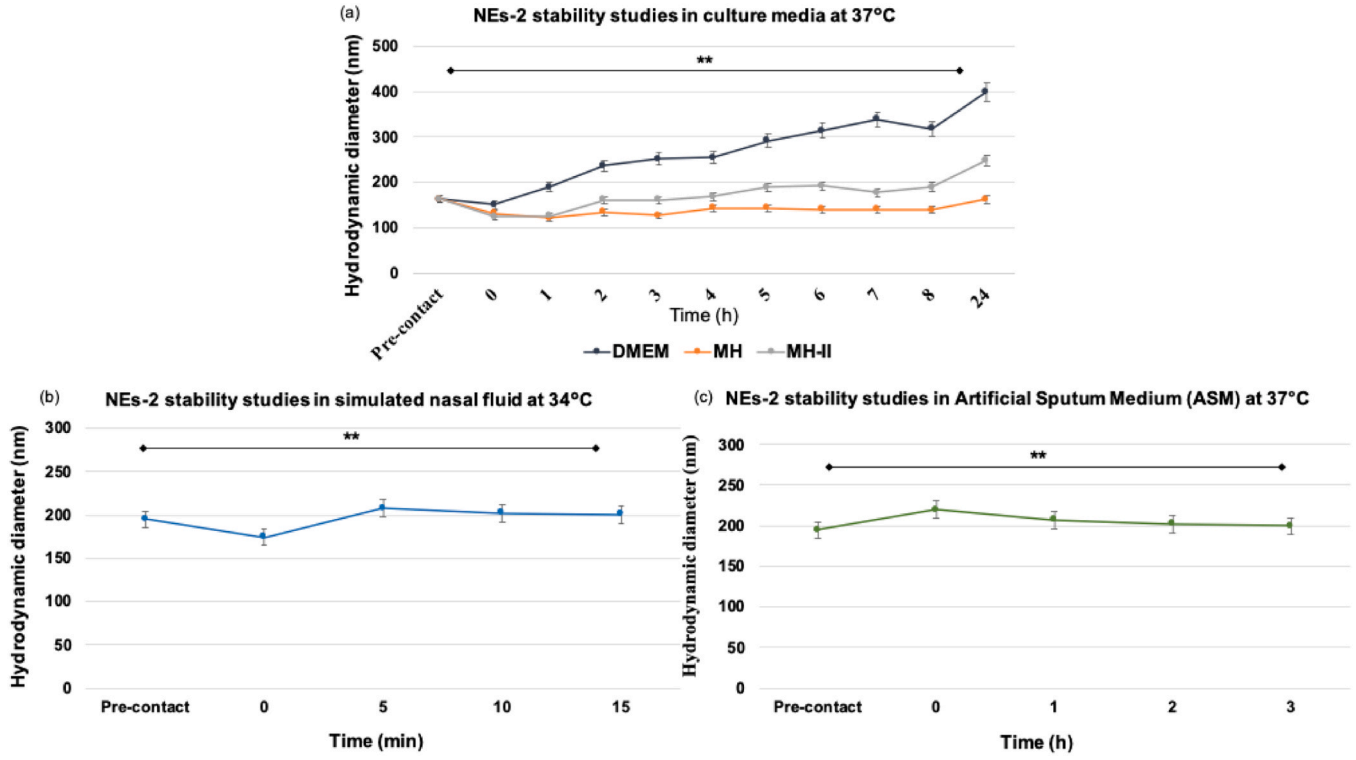

Fig. 10. . Effect of different culture media (DMEM, in blue, MH, in red and MH-II, in green, A), in simulated nasal fluid (B) and Artificial Sputum Medium (ASM) (C) at different incubation times on hydrodynamic diameter of NEs-2. Data were obtained as the mean of three independent experiments. * $p < 0.05$, * * $p < 0.01$, * ** $p < 0.001$.

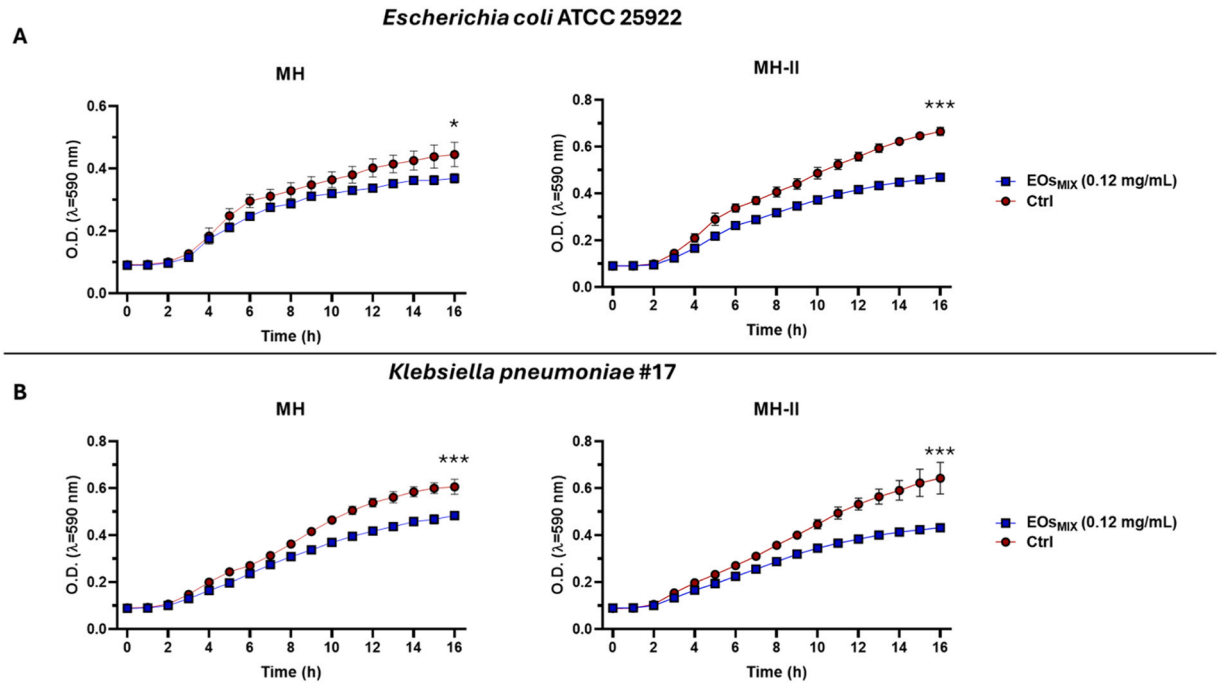

Fig. 11. . Effect of NEs-2 at the optimal concentration of EOsMIX, i.e., 0.12 mg/mL on the microbial growth (measured as optical density) of *E. coli* ATCC 25922 (panel A) and *K. pneumoniae* (panel B) in MH and MH-II. The data are the mean ± SD of three independent experiments. * $p < 0.05$, * ** $p < 0.001$.

Table 5
Physical-chemical characterization of samples in terms of hydrodynamic diameter, polydispersity index (PDI) and ζ-potential before and after nebulization process (pre and post, respectively).

Sample	Hydrodynamic diameter ± SD (nm)	PDI ± SD	ζ-potential ± SD (mV)
NEs−2 (pre)	178,00 ± 8,60	0,25 ± 0,01	−35,50 ±1,30
NEs−2 (post)	149,00 ± 2,60	0,26 ± 0,01	−31,40 ± 0,29

Through a multidisciplinary approach, it was possible to deeply characterize NEs-1 in terms of physical-chemical properties, antimicrobial activity and cytotoxicity.

NEs-1 was found to be not cytotoxic only at a concentration of $EOs_{MIX} = 0.12$ mg/mL, which also has a mild antimicrobial activity. The new optimized nanoemulsions (NEs-2) show no cytotoxic effect and antimicrobial activity. NEs-2 has been deeply characterized also by morphological analyses, and it showed similar physical-chemical properties compared to NEs-1, and resistance to biological simulated fluids. Moreover, preliminary studies on aerosolization were carried out and nebulized nanoemulsions, due to their specific features, could be able to reach the deeper regions of the lungs. In addition, NEs-2 was able to slow down the growth of two representative Gram-negative bacteria (i.e., *E. coli* and *K. pneumoniae*) without being cytotoxic against eukaryotic cells.

All in all, NEs-2 therefore represents an interesting example of a bioactive nanocarrier useful as a potential platform able to entrap drugs, antimicrobial molecules such as innovative antimicrobial peptides, to: (i) protect them from degradation; (ii) facilitate reaching the target size; (iii) potentiate their antimicrobial activity and (iv) reduce side effects due to their local administration.

CRediT authorship contribution statement

Floriana Cappiello: Investigation, Data curation. **Carlo Vetrano:** Investigation, Conceptualization. **Maria Gioia Fabiano:** Investigation, Data curation, Conceptualization. **Maria Carafa:** Writing – review & editing, Writing – original draft, Validation, Supervision, Conceptualization. **Maria Luisa Mangoni:** Writing – review & editing, Writing – original draft, Validation, Supervision, Conceptualization. **Carlotta Marianecci:** Writing – review & editing, Writing – original draft, Validation, Supervision, Conceptualization. **Jacopo Forte:** Writing – review & editing, Writing – original draft, Investigation, Funding acquisition, Data curation, Conceptualization. **Eleonora D′intino:** Writing – review & editing, Writing – original draft, Investigation, Data curation, Conceptualization. **Agnese Viscido:** Investigation. **Maria Grazia Ammendolia:** Investigation, Formal analysis, Data curation. **Bruno Casciaro:** Writing – review & editing, Writing – original draft, Validation, Supervision, Investigation, Data curation, Conceptualization. **Federica Rinaldi:** Writing – review & editing, Writing – original draft, Validation, Supervision, Investigation, Data curation, Conceptualization.

Declaration of Competing Interest

The authors declare that they have no known competing financial interests or personal relationships that could have appeared to influence the work reported in this paper.

Acknowledgements

This research was funded by Project ECS 00000024 Rome Technopole, - CUP B83C22002820006, PNRR Missione 4 Componente 2 Investimento 1.5, funded by European Union – NextGenerationEU and “Sapienza -Rome Technopole per l’Attrazione di early-career researchers MSCA Fellowship”, sviluppo presentato nell’ambito del Piano Nazionale di Ripresa e Resilienza - Missione 4 - Componente 2 - Investimento 1.5 - PE/CN -SPOKE 1 - (ECS 00000024). This research wa salso supported by Sapienza University (RM12117A5D5A92A4) (MLM).

Appendix A. Supporting information

Supplementary data associated with this article can be found in the

online version at doi:10.1016/j.colsurfb.2025.114733.

Data availability

Data will be made available on request.

References

[1] Md.A. Salam, Md.Y. Al-Amin, M.T. Salam, J.S. Pawar, N. Akhter, A.A. Rabaan, M. A.A. Alqumber, Antimicrobial resistance: a growing serious threat for global public health, Healthcare 11 (2023) 1946, https://doi.org/10.3390/healthcare11131946.

[2] C.J.L. Murray, K.S. Ikuta, F. Sharara, L. Swetschinski, G. Robles Aguilar, A. Gray, C. Han, C. Bisignano, P. Rao, E. Wool, S.C. Johnson, A.J. Browne, M.G. Chipeta, F. Fell, S. Hackett, G. Haines-Woodhouse, B.H. Kashef Hamadani, E.A.P. Kumaran, B. McManigal, S. Achalapong, R. Agarwal, S. Akech, S. Albertson, J. Amuasi, J. Andrews, A. Aravkin, E. Ashley, F.-X. Babin, F. Bailey, S. Baker, B. Basnyat, A. Bekker, R. Bender, J.A. Berkley, A. Bethou, J. Bielicki, S. Boonkasidecha, J. Bukosia, C. Carvalheiro, C. Castañeda-Orjuela, V. Chansamouth, S. Chaurasia, S. Chiurchiù, F. Chowdhury, R. Clotaire Donatien, A.J. Cook, B. Cooper, T. R. Cressey, E. Criollo-Mora, M. Cunningham, S. Darboe, N.P.J. Day, M. De Luca, K. Dokova, A. Dramowski, S.J. Dunachie, T. Duong Bich, T. Eckmanns, D. Eibach, A. Emami, N. Feasey, N. Fisher-Pearson, K. Forrest, C. Garcia, D. Garrett, P. Gastmeier, A.Z. Giref, R.C. Greer, V. Gupta, S. Haller, A. Haselbeck, S.I. Hay, M. Holm, S. Hopkins, Y. Hsia, K.C. Iregbu, J. Jacobs, D. Jarovsky, F. Javanmardi, A. W.J. Jenney, M. Khorana, S. Khusuwan, N. Kissoon, E. Kobeissi, T. Kostyanev, F. Krapp, R. Krumkamp, A. Kumar, H.H. Kyu, C. Lim, K. Lim, D. Limmathurotsakul, M.J. Loftus, M. Lunn, J. Ma, A. Manoharan, F. Marks, J. May, M. Mayxay, N. Mturi, T. Munera-Huertas, P. Musicha, L.A. Musila, M.M. Mussi-Pinhata, R.N. Naidu, T. Nakamura, R. Nanavati, S. Nangia, P. Newton, C. Ngoun, A. Novotney, D. Nwakanma, C.W. Obiero, T.J. Ochoa, A. Olivas-Martinez, P. Olliaro, E. Ooko, E. Ortiz-Brizuela, P. Ounchanum, G.D. Pak, J.L. Paredes, A.Y. Peleg, C. Perrone, T. Phe, K. Phommasone, N. Plakkal, A. Ponce-de-Leon, M. Raad, T. Ramdin, S. Rattanavong, A. Riddell, T. Roberts, J.V. Robotham, A. Roca, V.D. Rosenthal, K. E. Rudd, N. Russell, H.S. Sader, W. Saengchan, J. Schnall, J.A.G. Scott, S. Seekaew, M. Sharland, M. Shivamallappa, J. Sifuentes-Osornio, A.J. Simpson, N. Steenkeste, A.J. Stewardson, T. Stoeva, N. Tasak, A. Thaiprakong, G. Thwaites, C. Tigoi, C. Turner, P. Turner, H.R. Van Doorn, S. Velaphi, A. Vongpradith, M. Vongsouvath, H. Vu, T. Walsh, J.L. Walson, S. Waner, T. Wangrangsimakul, P. Wannapinij, T. Wozniak, T.E.M.W. Young Sharma, K.C. Yu, P. Zheng, B. Sartorius, A.D. Lopez, A. Stergachis, C. Moore, C. Dolecek, M. Naghavi, Global burden of bacterial antimicrobial resistance in 2019: a systematic analysis, Lancet 399 (2022) 629–655, https://doi.org/10.1016/S0140-6736(21)02724-0.

[3] X. Jin, J. Ren, R. Li, Y. Gao, H. Zhang, J. Li, J. Zhang, X. Wang, G. Wang, Global burden of upper respiratory infections in 204 countries and territories, 1990 2019, eClinicalMedicine 37 (2021) 100986, https://doi.org/10.1016/j.eclinm.2021.100986.

[4] E.J. Derbyshire, P.C. Calder, Respiratory tract infections and antibiotic resistance: a protective role for vitamin D? Front. Nutr. 8 (2021) 652469 https://doi.org/10.3389/fnut.2021.652469.

[5] Z. Breijyeh, B. Jubeh, R. Karaman, Resistance of gram-negative bacteria to current antibacterial agents and approaches to resolve it, Molecules 25 (2020) 1340, https://doi.org/10.3390/molecules25061340.

[6] A. Gauba, K.M. Rahman, Evaluation of antibiotic resistance mechanisms in gram-negative bacteria, Antibiotics 12 (2023) 1590, https://doi.org/10.3390/antibiotics12111590.

[7] L. Zhang, H. Bera, H. Wang, J. Wang, Y. Guo, C. Shi, D. Cun, C. Moser, N. Høiby, M. Yang, Combination and nanotechnology based pharmaceutical strategies for combating respiratory bacterial biofilm infections, Int. J. Pharm. 616 (2022) 121507, https://doi.org/10.1016/j.ijpharm.2022.121507.

[8] A.E. Edris, Pharmaceutical and therapeutic Potentials of essential oils and their individual volatile constituents: a review, Phytother. Res. 21 (2007) 308–323, https://doi.org/10.1002/ptr.2072.

[9] S. Chouhan, K. Sharma, S. Guleria, Antimicrobial activity of some essential oils—present status and future perspectives, Medicines 4 (2017) 58, https://doi.org/10.3390/medicines4030058.

[10] R. Bhattacharya, R. Rolta, K. Dev, A. Sourirajan, Synergistic potential of essential oils with antibiotics to combat fungal pathogens: present status and future perspectives, Phytother. Res. 35 (2021) 6089–6100, https://doi.org/10.1002/ptr.7218.

[11] R. Tao, J. Sedman, A. Ismail, Antimicrobial activity of various essential oils and their application in active packaging of frozen vegetable products, Food Chem. 360 (2021) 129956, https://doi.org/10.1016/j.foodchem.2021.129956.

[12] T.A. Wani, F.A. Masoodi, S.M. Jafari, D.J. McClements, Safety of Nanoemulsions and Their Regulatory Status. in: Nanoemulsions, Elsevier, 2018, pp. 613–628, 10.1016/B978-0-12-811838-2.00019-9.

[13] A. Maurya, V.K. Singh, S. Das, J. Prasad, A. Kedia, N. Upadhyay, N.K. Dubey, A. K. Dwivedy, Essential oil nanoemulsion as eco-friendly and safe preservative: bioefficacy against microbial food deterioration and toxin secretion, mode of action, and future opportunities, Front. Microbiol. 12 (2021) 751062, https://doi.org/10.3389/fmicb.2021.751062.

[14] R. Mokhtari, M. Kazemi Fard, M. Rezaei, S.A. Moftakharzadeh, A. Mohseni, Antioxidant, antimicrobial activities, and characterization of phenolic compounds of thyme (Thymus vulgaris L.), sage (Salvia officinalis L.), and thyme–sage mixture extracts, J. Food Qual. 2023 (2023) 1–9, https://doi.org/10.1155/2023/2602454.

[15] A. Manilal, K.R. Sabu, M. Woldemariam, A. Aklilu, G. Biresaw, T. Yohanes, M. Seid, B. Merdekios, Antibacterial activity of rosmarinus officinalis against multidrug-resistant clinical isolates and meat-borne pathogens, Evid. -Based Complement. Altern. Med. 2021 (2021) 1–10, https://doi.org/10.1155/2021/6677420.

[16] A.R. Blanc, M.A. Sortino, E. Butassi, L.A. Svetaz, Synergistic effects of Thymus vulgaris essential oil in combination with antifungal agents and inhibition of virulence factors of Candida albicans, Phytomedicine 3 (2023) 100481, https://doi.org/10.1016/j.phyplu.2023.100481.

[17] O. Amassmoud, I. Abbad, M. Iriti, L. Hassani, N. Mezrioui, A. Abbad, Antibacterial activity of essential oils combinations based on thymus broussonnetii, and their synergism with some antibiotics, Curr. Microbiol 80 (2023) 398, https://doi.org/10.1007/s00284-023-03510-x.

[18] S. Peng, W. Wang, R. Zhang, C. Wu, X. Pan, Z. Huang, Nano-formulations for pulmonary delivery: past, present, and future perspectives, Pharmaceutics 16 (2024) 161, https://doi.org/10.3390/pharmaceutics16020161.

[19] H. Miladi, R.B. Slama, D. Mili, S. Zouari, A. Bakhrouf, E. Ammar, Essential oil of <i>Thymus vulgaris< /i> L. and <i>Rosmarinus officinalis< /i> L.: Gas chromatography-mass spectrometry analysis, cytotoxicity and antioxidant properties and antibacterial activities against foodborne pathogens, NS 05 (2013) 729–739, https://doi.org/10.4236/ns.2013.56090.

[20] A.P. Ramos, Dynamic Light Scattering Applied to Nanoparticle Characterization. in:Nanocharacterization Techniques, Elsevier, 2017, pp. 99–110, 10.1016/B978-0-323-49778-7.00004-7.

[21] F. Rinaldi, P.N. Hanieh, S. Sennato, F.D. Santis, J. Forte, M. Fraziano, S. Casciardi, C. Marianecci, F. Bordi, M. Carafa, Rifampicin–Liposomes for Mycobacterium abscessus Infection Treatment: Intracellular Uptake and Antibacterial Activity Evaluation2021.

[22] H. Tanigawa, N. Suzuki, T. Suzuki, Application of ionic liquid to enhance the nose-to-brain delivery of etodolac, Eur. J. Pharm. Sci. 178 (2022) 106290, https://doi.org/10.1016/j.ejps.2022.106290.

[23] C. Marianecci, L.D. Marzio, F. Rinaldi, M. Carafa, F. Alhaique, Pulmonary delivery: innovative approaches and perspectives, JBNB 02 (2011) 567–575, https://doi.org/10.4236/jbnb.2011.225068.

[24] P. Muralidharan, M. Malapit, E. Mallory, D. Hayes, H.M. Mansour, Inhalable nanoparticulate powders for respiratory delivery, Nanomed.: Nanotechnol., Biol. Med. 11 (2015) 1189–1199, https://doi.org/10.1016/j.nano.2015.01.007.

[25] Z. Németh, I. Csóka, R. Semnani Jazani, B. Sipos, H. Haspel, G. Kozma, Z. Kónya, D. G. Dobó, Quality by design-driven zeta potential optimisation study of liposomes with charge imparting membrane additives, Pharmaceutics 14 (2022) 1798, https://doi.org/10.3390/pharmaceutics14091798.

[26] L. Maurizi, A. Lasalvia, M.G. Fabiano, E. D'Intino, F. Del Cioppo, C. Fraschetti, A. Filippi, M.G. Ammendolia, A.L. Conte, J. Forte, D. Corinti, M.E. Crestoni, M. Carafa, C. Marianecci, F. Rinaldi, C. Longhi, Lentisk (pistacia lentiscus) oil nanoemulsions loaded with levofloxacin: phytochemical profiles and antibiofilm activity against Staphylococcus spp, Pharmaceutics 16 (2024) 927, https://doi.org/10.3390/pharmaceutics16070927.

[27] P.C. Soema, G.-J. Willems, W. Jiskoot, J.-P. Amorij, G.F. Kersten, Predicting the influence of liposomal lipid composition on liposome size, zeta potential and liposome-induced dendritic cell maturation using a design of experiments approach, Eur. J. Pharm. Biopharm. 94 (2015) 427–435, https://doi.org/10.1016/j.ejpb.2015.06.026.

[28] L. Maurizi, J. Forte, M.G. Ammendolia, P.N. Hanieh, A.L. Conte, M. Relucenti, O. Donfrancesco, C. Ricci, F. Rinaldi, C. Marianecci, M. Carafa, C. Longhi, Effect of ciprofloxacin-loaded niosomes on escherichia coli and staphylococcus aureus biofilm formation, Pharmaceutics 14 (2022) 2662, https://doi.org/10.3390/pharmaceutics14122662.

[29] M. Danaei, M. Dehghankhold, S. Ataei, F. Hasanzadeh Davarani, R. Javanmard, A. Dokhani, S. Khorasani, M.R. Mozafari, Impact of particle size and polydispersity index on the clinical applications of lipidic nanocarrier systems, Pharmaceutics 10 (2018) 57, https://doi.org/10.3390/pharmaceutics10020057.

[30] N. Keksel, H. Bussmann, M. Unger, J. Drewe, G. Boonen, H. Häberlein, S. Franken, St John's wort extract influences membrane fluidity and composition of phosphatidylcholine and phosphatidylethanolamine in rat C6 glioblastoma cells, Phytomedicine 54 (2019) 66–76, https://doi.org/10.1016/j.phymed.2018.06.013.

[31] M. Amararathna, K. Goralski, D. Hoskin, H.P. Rupasinghe, Pulmonary nano-drug delivery systems for lung cancer: current knowledge and prospects, J. Lung Health Dis. 3 (2019) 11–28, https://doi.org/10.29245/2689-999X/2019/2.1148.

[32] J.L. Purdie, R.L. Kowle, A.L. Langland, C.N. Patel, A. Ouyang, D.J. Olson, Cell culture media impact on drug product solution stability, Biotechnol. Prog. 32 (2016) 998–1008, https://doi.org/10.1002/btpr.2289.

[33] R. Russo, M.T. Corasaniti, G. Bagetta, L.A. Morrone, Exploitation of cytotoxicity of some essential oils for translation in cancer therapy, Evid. -Based Complement. Altern. Med. 2015 (2015) 1–9, https://doi.org/10.1155/2015/397821.

[34] M. Ganguly, D. Debraj, N. Mazumder, J. Carpenter, S. Manickam, A.B. Pandit, Impact of ultrasonication on the oxidative stability of oil-in-water nanoemulsions: investigations into kinetics and strategies to control lipid oxidation, Ind. Eng. Chem. Res. 63 (2024) 10212–10225, https://doi.org/10.1021/acs.iecr.4c00506.

[35] R. Bnyan, I. Khan, T. Ehtezazi, I. Saleem, S. Gordon, F. O'Neill, M. Roberts, Surfactant effects on lipid-based vesicles properties, J. Pharm. Sci. 107 (2018) 1237–1246, https://doi.org/10.1016/j.xphs.2018.01.005.

[36] R.R. Patlolla, M. Chougule, A.R. Patel, T. Jackson, P.N.V. Tata, M. Singh, Formulation, characterization and pulmonary deposition of nebulized celecoxib encapsulated nanostructured lipid carriers, J. Control. Release 144 (2010) 233–241, https://doi.org/10.1016/j.jconrel.2010.02.006.